


## RESEARCH ARTICLE

# Element differential method and its application in thermal-mechanical problems

Xiao-Wei Gao  | Zong-Yang Li | Kai Yang | Jun Lv | Hai-Feng Peng | Miao Cui | Bo Ruan | Qiang-Hua Zhu

State Key Laboratory of Structural Analysis for Industrial Equipment, Dalian University of Technology, Dalian 116024, China

## Correspondence

Xiao-Wei Gao, State Key Laboratory of Structural Analysis for Industrial Equipment, Dalian University of Technology, Dalian 116024, China.

Email: xwgao@dlut.edu.cn

## Funding information

National Natural Science Foundation of China, Grant/Award Number: 11302040, 11572075 and 11672061

## Summary

In this paper, a new numerical method, element differential method (EDM), is proposed for solving general thermal-mechanical problems. The key point of the method is the direct differentiation of the shape functions of Lagrange isoparametric elements used to characterize the geometry and physical variables. A set of analytical expressions for computing the first- and second-order partial derivatives of the shape functions with respect to global coordinates are derived. Based on these expressions, a new collocation method is proposed for establishing the system of equations, in which the equilibrium equations are collocated at nodes inside elements, and the traction equilibrium equations are collocated at interface nodes between elements and outer surface nodes of the problem. Attributed to the use of the Lagrange elements that can guarantee the variation of physical variables consistent through all elemental nodes, EDM has higher stability than the traditional collocation method. The other main features of EDM are that no mathematical or mechanical principles are required to set up the system of equations and no integrals are involved to form the coefficients of the system. A number of numerical examples of 2- and 3-dimensional problems are given to demonstrate the correctness and efficiency of the proposed method.

## KEYWORDS

BEM, element differential method (EDM), FEM, Lagrange isoparametric elements, shape functions, thermal-mechanical problems

## 1 | INTRODUCTION

In mathematics, the thermal-mechanical problem is one of the boundary value problems of the second-order partial differential equations (PDEs). The key task to solve this type of PDEs is to treat the involved second-order partial derivatives of related physical variables with respect to the global coordinates. A number of successful numerical methods are available to do this, which can be classified into 2 types: the weak-form technique and the strong-form technique.<sup>1</sup>

In the weak-form technique, the frequently used methods are the finite element method (FEM),<sup>2-8</sup> boundary element method (BEM),<sup>9-22</sup> finite volume method (FVM),<sup>23-26</sup> and a part of mesh free methods (MFM).<sup>27-33</sup> In this technique, the spatially partial derivatives of physical variables appearing in the governing PDEs are converted into some terms, including the physical variables and their lower orders of derivatives based on a mathematical principle, eg, the variational principle, or a mechanical principle, eg, the energy principle.<sup>2,4</sup> Usually, the resulted weak form of the problem involves some integrals over a series of

elements used to discretize the geometry of the problem and interpolate-related physical variables. Attributing to the use of well-formed elements that can guarantee the variation of the physical variables to be consistent through element nodes, the weak-form technique usually results in very stable computational results.

The strong-form technique mainly includes the point collocation methods,<sup>34,35</sup> most part approaches of MFM,<sup>1,33,36</sup> and the conventional finite difference method (FDM).<sup>37-41</sup> In this technique, a number of nodes around the node under consideration are selected locally to form a certain order of array. The global spatial derivatives of physical variables are calculated using the so called “shape functions” constructed by the selected array of points. Moreover, the final system of equations can be formed by directly substituting the expressions of calculating the spatial derivatives into the governing PDEs and the boundary conditions. Because all the equations (governing equations and boundary conditions) are enforced at the nodes, this type of technique is usually called the collocation method.<sup>31,42</sup> The working process of this method is very straightforward and can be easily coded for complicated multi-field problems. However, because there are no means to control the stability and the convergence of the solution, the collocation method is often found not stable and the solutions can vary a lot when the location and distribution of nodes are changed.<sup>1</sup> Besides, because the governing equation and the boundary conditions are entirely separately satisfied at individual nodes, there could be conflicts for nodes near the boundaries.<sup>1</sup> This disconnected situation could be one of the main causes of the instability issues with the collocation method. Therefore, certain stabilization techniques must be used in this type of strong-form techniques.<sup>27</sup>

The above-mentioned methods have been successfully used to solve various engineering problems and different advantages and drawbacks can be summarized for these methods. FVM and FDM are the frequently used methods in fluid mechanics as well as in heat and mass transfer problems. They have the advantages of easily discretizing the governing equations and treating discontinuous physical phenomena,<sup>23</sup> such as capturing shock waves and implementing upwind scheme. The main drawback of these 2 methods is that a lot of control volumes or points are required to achieving a satisfactory result, and the computational accuracy in heat flux on the boundary is poor.<sup>43-45</sup> Besides, FDM is awkward when working in body-fitted coordinates. FEM is the dominant method in the analysis of solid mechanics as well as other engineering problems. The distinct advantage of FEM is in its flexibility and applicability. Almost any engineering problems can be solved using FEM. This feature is attributed to the use of various well-formed isoparametric elements which can be used to discretize the geometry of the problem and interpolate physical variables. Moreover, also because of using the isoparametric elements, the total numbers of elements and nodes required in FEM are much less than those used in FVM and FDM. The drawbacks of FEM are mainly embodied in that a variational or a virtual work principle is needed to establish the FEM algorithm<sup>2-4</sup> and the resulted integrals need to be evaluated over the discretized elements. Comparing to FEM, BEM only needs to discretize the boundary of the problem into elements, which not only can reduce the dimensions of the problem but also can easily simulate the stress concentration behaviors.<sup>9,14</sup> One of the drawbacks of BEM is that the fundamental solutions are derived from linear problems,<sup>12,16</sup> and therefore it is difficult to establish a pure BEM algorithm for nonlinear and nonhomogeneous problems.<sup>14,18</sup> Different from these mesh-dependent methods, MFM only needs a group of distributed points in the computational domain. Therefore, the distinct advantage of MFM is that problems with irregular geometries can be easily simulated. However, MFM has the drawbacks of time consuming to form the global shape functions and difficulty to apply boundary conditions.<sup>27,28</sup>

Recently, a different strong-form technique is proposed by Wen and Li,<sup>46-48</sup> which is called the finite block method (FBM). In this method, isoparametric element-like blocks are used to compute the first-order partial derivative of physical variables with respect to the global coordinates. As other strong-form techniques, FBM has the advantage of easily coding, and because the element-like blocks are used, the stability of the solution is usually excellent. On the other hand, because all nodal physical variables over each block are independently put in the system of equations, the unknowns of the formed final system of equations are much more than other frequently used numerical methods under the case of the same number of total nodes. Because of this reason, when solving a problem using FBM, as few blocks as possible are used to reduce the number of interface nodes between blocks and thus ensure the final system of equation is not so huge. When solving a larger problem, high-order blocks (each having many nodes) need to be used to ensure the computational accuracy. Besides, because the second-order partial derivatives (which are the typical terms in most governing equations of engineering problems) are calculated through the recursive use of the first-order derivative formulation, the computational accuracy could be lower than using the analytical expressions of high-order derivatives as derived in this paper.

In this paper, a new robust method, element differential method (EDM),<sup>49</sup> is proposed for solving general boundary value problems of the second-order PDEs based on the use of Lagrange isoparametric elements as used in the standard FEM.<sup>2</sup> A set of explicit formulations of computing the first- and second-order spatial derivatives are derived for 2-dimensional (2D) and 3-dimensional (3D) problems. These formulations are expressed through shape functions of elements and therefore can be used for any physical variables' differentiation. EDM is a strong-form technique, which borrows the idea

of FEM in the aspect of using isoparametric elements to obtain spatial derivatives and the idea of FBM and collocation-like MFM in the aspect of collocating equations at nodes. The former (using elements) can result in very stable solutions and the latter (collocating at nodes) does not require any integration. Two distinct novelties can be stated here for the paper. The first one is that a set of analytical expressions of computing the second-order spatial derivatives of the shape functions of any orders of Lagrange elements are derived for the first time, which can make the computation more accurate and faster. The second one is that a new collocation and system-assembling technique, the traction equilibrium technique, is proposed for forming the system of equations, which can make the final system smaller and therefore suitable for solving large-scale engineering problems. The important feature of the proposed method is that the derived spatial derivatives can be directly substituted into the governing equations and the boundary conditions to form the final system of algebraic equations, and therefore EDM is very easy to be coded and implemented in dealing with problems with complicated governing equations and boundary conditions.

## 2 | GOVERNING EQUATIONS FOR THERMAL-MECHANICAL PROBLEMS

The differential equation for steady thermal-mechanical problems is described by the following equilibrium equation [17]:

$$\frac{\partial \sigma_{ij}(x)}{\partial x_j} + b_i(x) = 0, \quad x \in \Omega, \quad (1)$$

where  $\sigma_{ij}$  is the stress tensor,  $b_i$  is the body force,  $\Omega$  is the computational domain, and the repeated index  $j$  stands for the summation.

The stress tensor  $\sigma_{ij}$  can be expressed in terms of the strain tensor  $\varepsilon_{kl}$  and the temperature  $T$  through the following constitutive relationship<sup>17</sup>:

$$\sigma_{ij} = D_{ijkl}\varepsilon_{kl} - \tilde{k}T\delta_{ij}, \quad (2)$$

where

$$\varepsilon_{kl} = \frac{1}{2} \left( \frac{\partial u_k}{\partial x_l} + \frac{\partial u_l}{\partial x_k} \right), \quad (3)$$

$$D_{ijkl} = \lambda \delta_{ij}\delta_{kl} + \mu(\delta_{ik}\delta_{jl} + \delta_{il}\delta_{jk}), \quad (4a)$$

$$\lambda = \frac{2\mu\nu}{(1-2\nu)}, \quad (4b)$$

$$\tilde{k} = \frac{2\mu(1+\nu)}{1-2\nu}k. \quad (4c)$$

In these equations,  $\mu$  is the shear modulus,  $\nu$  is the Poisson ration,  $k$  is the coefficient of thermal expansion, and  $D_{ijkl}$  is the elasticity constitutive tensor with the symmetry of  $D_{ijkl} = D_{jikl} = D_{ijlk} = D_{klij}$ .

Traction  $t_i$  on the surface  $\Gamma$  of the problem can be related to the stress tensor  $\sigma_{ij}$  through the following relationship:

$$t_i = \sigma_{ij}n_j, \quad (5)$$

where  $n_j$  is the outward normal vector to the surface  $\Gamma$ .

By substituting Equation 3 into Equations 2 and 5 and the results into Equation 1, the boundary value problem in the thermal-mechanical analysis can be described by the following second-order PDE:

$$D_{ijkl}(x) \frac{\partial^2 u_k(x)}{\partial x_l \partial x_j} + \frac{\partial D_{ijkl}(x)}{\partial x_j} \frac{\partial u_k(x)}{\partial x_l} - \frac{\partial(\tilde{k}(x)T(x))}{\partial x_i} + b_i(x) = 0, \quad x \in \Omega, \quad (6)$$

and the following boundary conditions:

$$u_i(x) = \bar{u}_i(x), \quad x \in \Gamma_u, \quad (7a)$$

$$t_i(x) = D_{ijkl}(x)n_j(x)\frac{\partial u_k(x)}{\partial x_l} - \tilde{k}(x)T(x)n_i(x) = \bar{t}_i(x), \quad x \in \Gamma_t, \quad (7b)$$

where  $\Gamma_u$  and  $\Gamma_t$  are the boundaries specified by the displacement  $\bar{u}_i$  and the traction  $\bar{t}_i$ , respectively, with  $\Gamma_u \cup \Gamma_t = \Gamma$ .

It is noted that the governing Equation 6 and the traction-displacement relationship 7b can account for the cases of varying material coefficients such as in the nonhomogeneous and nonlinear problems.

### 3 | DERIVATIVES OF ELEMENTAL SHAPE FUNCTIONS WITH RESPECT TO GLOBAL COORDINATES

From Equations 6 and 7, it can be seen that the key task to solve the thermal-mechanical problems is to establish an algorithm to compute the first- and second-order partial derivatives of the physical variables, such as the displacement and temperature, with respect to global spatial coordinates. The isoparametric elements used in FEM<sup>2,3</sup> have excellent characteristics in geometry representation and physical variable interpolation. The essential work of this paper is to derive a set of analytical expressions for computing the first- and second-order partial derivatives needed in solving the PDEs based on Lagrange isoparametric elements.

#### 3.1 | Shape functions of Lagrange isoparametric elements

To numerically compute the partial derivatives appearing in Equations 6 and 7, the Lagrange isoparametric elements<sup>2,3</sup> are adopted herein. The key mathematical quantities characterizing the isoparametric elements are the shape functions used to model the geometry and interpolate physical variables. The shape functions for 1D isoparametric elements can be determined by the Lagrange interpolation formulation:

$$L_I^m(\xi) = \prod_{i=1, i \neq I}^m \frac{\xi - \xi_i}{\xi_I - \xi_i} \quad (I = 1 \sim m, \quad -1 \leq \xi \leq 1), \quad (8)$$

where  $m$  is the number of interpolation points, and  $\xi$  is the isoparametric coordinate (also called the intrinsic or natural coordinate). For example, the shape functions for a 3-node line element (Figure 1) can be expressed as follows:

$$\begin{cases} L_1^3(\xi) = -\frac{1}{2}\xi(1-\xi) \\ L_2^3(\xi) = 1-\xi^2 \\ L_3^3(\xi) = \frac{1}{2}\xi(1+\xi) \end{cases}. \quad (9)$$

##### 3.1.1 | Shape functions for 2D and 3D Lagrange isoparametric elements

The shape functions for 2D and 3D problems can be formed based on the 1D shape functions shown in Equation 8. The rule of forming 2D and 3D shape functions can be found in the studies of Zienkiewicz and Taylor<sup>2</sup> and Hughes,<sup>3</sup> which can be expressed as follows:

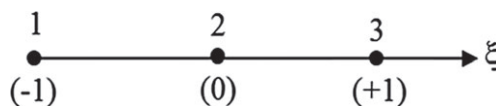


FIGURE 1 Three-node line element

$$N_{\alpha}(\xi, \eta) = L_I^m(\xi)L_J^n(\eta) \quad (10)$$

for 2D elements, and

$$N_{\alpha}(\xi, \eta, \zeta) = L_I^m(\xi)L_J^n(\eta)L_K^p(\zeta) \quad (11)$$

for 3D elements.

In Equations 10 and 11, the superscripts  $m$ ,  $n$ , and  $p$  are the numbers of the interpolation points along  $\xi$ ,  $\eta$ , and  $\zeta$  directions, respectively, and the subscript  $\alpha$  is determined by the permutation of the subscripts  $I$ ,  $J$ , and  $K$  sequentially. Figure 2 shows the 9-node 2D quadrilateral element generated using Equation 10 by setting  $m = 3$  and  $n = 3$ , whereas Figure 3 shows the 27-node 3D brick element generated using Equation 11 by setting  $m = 3$ ,  $n = 3$ , and  $p = 3$ . As an example of the 9-node 2D element as shown in Figure 2, the shape functions  $N_2$  and  $N_5$  can be formed as  $N_2(\xi, \eta) = L_2^3(\xi)L_1^3(\eta)$  and  $N_5(\xi, \eta) = L_2^3(\xi)L_2^3(\eta)$ .

### 3.1.2 | Expressing coordinates and physical variables in terms of element nodal values

Any variables varying over an isoparametric element can be expressed in terms of their nodal values of the element.<sup>2</sup> For example, the spatial coordinates and displacements can be expressed as

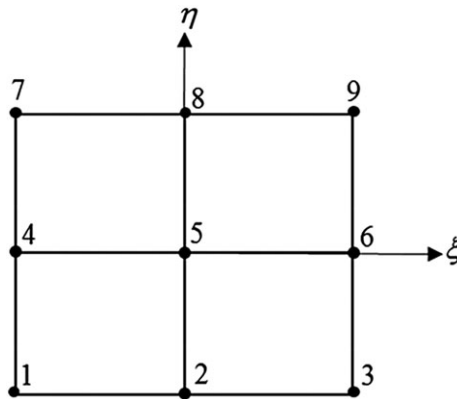


**FIGURE 2** Nine-node 2D quadrilateral element

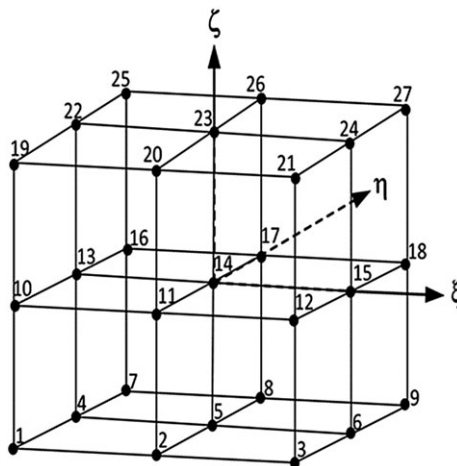


**FIGURE 3** Twenty-seven-node 3D brick element

$$x_i = N_\alpha x_i^\alpha, \quad (12a)$$

$$u_i = N_\alpha u_i^\alpha, \quad (12b)$$

where  $x_i^\alpha$  and  $u_i^\alpha$  are the values of coordinates and displacements at node  $\alpha$ , and the repeated index  $\alpha$  represents the summation over all elemental nodes.

### 3.2 | Derivatives of shape functions with respect to global coordinates

To numerically compute the partial derivatives appearing in the governing Equation 6 and the boundary conditions in Equation 7, the analytical expressions for the first and second partial derivatives need to be derived. To do this, differentiating Equation 12b yields

$$\begin{aligned} \frac{\partial u_k}{\partial x_i} &= \frac{\partial N_\alpha}{\partial x_i} u_k^\alpha \\ \frac{\partial^2 u_k}{\partial x_i \partial x_j} &= \frac{\partial^2 N_\alpha}{\partial x_i \partial x_j} u_k^\alpha. \end{aligned} \quad (13)$$

From Equations 10 and 11, it can be seen that  $N_\alpha$  are the explicit functions of intrinsic coordinates  $\xi_k$ ; thus,

$$\frac{\partial N_\alpha}{\partial x_i} = \frac{\partial N_\alpha}{\partial \xi_k} \frac{\partial \xi_k}{\partial x_i} = [J]_{ik}^{-1} \frac{\partial N_\alpha}{\partial \xi_k}, \quad (14)$$

$$\frac{\partial^2 N_\alpha}{\partial x_i \partial x_j} = \left[ [J]_{ik}^{-1} \frac{\partial^2 N_\alpha}{\partial \xi_k \partial \xi_l} + \frac{\partial [J]_{ik}^{-1}}{\partial \xi_l} \frac{\partial N_\alpha}{\partial \xi_k} \right] \frac{\partial \xi_l}{\partial x_j}, \quad (15)$$

where  $[J] = [\partial x / \partial \xi]$  is the Jacobian matrix mapping from the global coordinate system  $x_i$  to the intrinsic coordinate system  $\xi_k$ , with  $(x_1, x_2) = (x, y)$  and  $(\xi_1, \xi_2) = (\xi, \eta)$  for 2D problems, and  $(x_1, x_2, x_3) = (x, y, z)$  and  $(\xi_1, \xi_2, \xi_3) = (\xi, \eta, \varsigma)$  for 3D problems. The  $\partial \xi_l / \partial x_j$  in Equations 14 and 15 can be determined by the following matrix relationship<sup>2</sup>:

$$\left[ \frac{\partial \xi}{\partial x} \right] = [J]^{-1} = \left[ \frac{\partial x}{\partial \xi} \right]^{-1}, \quad (16)$$

where

$$\left[ \frac{\partial x}{\partial \xi} \right]_{ik} = \frac{\partial x_i}{\partial \xi_k} = \frac{\partial N_\alpha}{\partial \xi_k} x_i^\alpha. \quad (17)$$

The inverse matrix of the Jacobian matrix  $[J]$  in Equation 16 can be written as the following form:

$$[J]^{-1} = \frac{1}{|J|} [A], \quad (18)$$

where

$$[A] = \begin{bmatrix} y_\eta & -y_\xi \\ -x_\eta & x_\xi \end{bmatrix}, \quad (19)$$

$$|J| = x_\xi y_\eta - x_\eta y_\xi, \quad (20)$$

for 2D problems, and

$$[A] = \begin{bmatrix} y_\eta z_\xi - y_\xi z_\eta & y_\xi z_\xi - y_\xi z_\xi & y_\xi z_\eta - y_\eta z_\xi \\ x_\xi z_\eta - x_\eta z_\xi & x_\xi z_\xi - x_\xi z_\xi & x_\eta z_\xi - x_\xi z_\eta \\ x_\eta y_\xi - x_\xi y_\eta & x_\xi y_\xi - x_\xi y_\xi & x_\xi y_\eta - x_\eta y_\xi \end{bmatrix}, \quad (21)$$

$$|J| = x_\xi y_\eta z_\xi - x_\eta y_\xi z_\xi - x_\xi y_\xi z_\eta + x_\xi y_\xi z_\eta + x_\eta y_\xi z_\xi - x_\xi y_\eta z_\xi, \quad (22)$$

for 3D problems.

In above equations,  $z_\eta = \partial z / \partial \eta = (\partial N_\alpha / \partial \eta) z^\alpha$ , and the same meaning can be applied to other terms.

Thus, differentiating Equation 18 leads to

$$\frac{\partial [J]^{-1}}{\partial \xi_k} = \frac{1}{|J|} \frac{\partial [A]}{\partial \xi_k} - \frac{1}{|J|^2} \frac{\partial |J|}{\partial \xi_k} [A]. \quad (23)$$

For 2D problems, it can be easily derived from Equations 19 and 20 that

$$\frac{\partial [A]}{\partial \xi} = \begin{bmatrix} y_{\eta\xi} & -y_{\xi\xi} \\ -x_{\eta\xi} & x_{\xi\xi} \end{bmatrix}, \quad (24a)$$

$$\frac{\partial [A]}{\partial \eta} = \begin{bmatrix} y_{\eta\eta} & -y_{\xi\eta} \\ -x_{\eta\eta} & x_{\xi\eta} \end{bmatrix}, \quad (24b)$$

$$\frac{\partial |J|}{\partial \xi} = x_{\xi\xi} y_\eta + x_\xi y_{\eta\xi} - x_{\eta\xi} y_\xi - x_\eta y_{\xi\xi}, \quad (25a)$$

$$\frac{\partial |J|}{\partial \eta} = x_{\xi\eta} y_\eta + x_\xi y_{\eta\eta} - x_{\eta\eta} y_\xi - x_\eta y_{\xi\eta}. \quad (25b)$$

For 3D problems, the expressions are a little bit complicated and have been given in Appendix A.

The terms  $\frac{\partial N_\alpha}{\partial \xi_k}$  and  $\frac{\partial^2 N_\alpha}{\partial \xi_k \partial \xi_l}$  in Equations 14 and 15 can be easily obtained by directly differentiating Equation 10 for 2D or Equation 11 for 3D problems.

Using the above-mentioned analytical expressions, the first- and second-order spatial derivatives of the shape functions with respect to global coordinates can be computed, and a system of equations can be formed by substituting these derivatives into the governing equation and boundary conditions.

## 4 | ASSEMBLING THE SYSTEM OF EQUATIONS BASED ON GOVERNING EQUATIONS AND TRACTION EQUILIBRIUM CONDITIONS

When solving a thermal-mechanical problem governed by the PDEs as shown in Equations 6 and 7 using EDM, the computational domain  $\Omega$  needs to be discretized into a series of elements in the similar way to FEM. A set of global nodes are defined sequentially through the entire computational domain, and a connection array is used to link the element nodes and the global nodes. The system of equations is established using a collocation scheme at each global node. The first and the second spatial derivatives of physical variables are computed using Equations 13–15 for each element, including the collocation node under consideration. Moreover, the final system of equations can be directly formed by assembling each element's contribution to the system through the connection array. Because the assembling manner is different for different positions of the collocation node located over an element, 3 types of nodes are defined for internal, interface and outer surface nodes, as shown in Figure 4 for a problem consisting of four 9-node elements. The internal nodes refer to the nodes completely located within elements, and the interface nodes refer to the nodes shared by a number of elements, whereas the outer surface nodes refer to the nodes located on the out boundary of the problem.

The collocation method proposed in this paper is different from the traditional ones. In the traditional collocation method (TCM), the equilibrium equations are usually collocated at all nodes inside the problem, whereas the boundary conditions

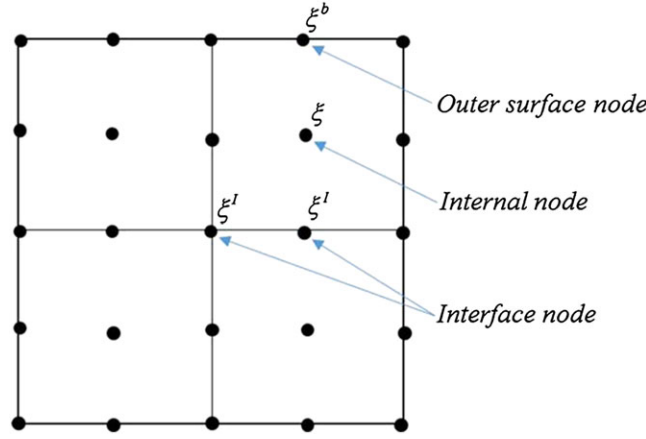


**FIGURE 4** Three types of nodes

are collocated at the nodes on the problem boundary. In the present method, the equilibrium equations are collocated only at the nodes inside elements, and the traction equilibrium equations are collocated at the interface nodes between the elements and the outer surface nodes of the problem. To clearly understand the proposed method, 4 and 6 surfaces over a 2D and 3D element, respectively, are also defined in the paper. Figure 5 shows the 4 surfaces of the 2D 9-node element, in which surfaces 1–4 are respectively defined over the bottom, right, top, and left sides of the element.

The detailed description of the present collocation method is given in the following subsections.

#### 4.1 | Setting up equations for internal nodes of elements based on the equilibrium equation

For nodes located within an element, the governing Equation 6 should be satisfied. Thus, by substituting Equation 13 into Equation 6, it follows that

$$\left[ D_{ijkl}(\xi) \frac{\partial^2 N_\alpha(\xi)}{\partial x_i \partial x_j} + \frac{\partial N_\beta(\xi)}{\partial x_j} D_{ijkl}^\beta \frac{\partial N_\alpha(\xi)}{\partial x_l} \right] u_k^\alpha - \frac{\partial N_\alpha(\xi)}{\partial x_i} \tilde{k}^\alpha T^\alpha + b_i(\xi) = 0, \quad \xi \in \Omega_e, \quad (26)$$

where  $\xi$  is the intrinsic coordinate at the node inside an element, say element  $e$ , under considered (see Figure 6), with  $\xi = (\xi, \eta)$  for 2D, and  $\xi = (\xi, \eta, \zeta)$  for 3D problems. For each element internal node, we can set up an equation using Equation 26, which is formulated in terms of the element nodal values of displacement.

#### 4.2 | Setting up equations for element interface nodes based on traction equilibrium conditions

For a node located on the interface shared by a few elements, the relationship between the traction and the displacement, ie, Equation 7b, is applied to each surface, including the node. In terms of the traction equilibrium condition  $\sum_{e=1}^{N^I} \sum_{s=1}^{S^{eI}} t_i^s(\xi^{eI}) = 0$  on the interface, the following equation can be set up by substituting Equation 13 into Equation 7b:

$$\sum_{e=1}^{N^I} \sum_{s=1}^{S^{eI}} \left[ D_{ijkl}(\xi^{eI}) n_j^s(\xi^{eI}) \frac{\partial N_\alpha(\xi^{eI})}{\partial x_l} u_k^\alpha - \tilde{k}(\xi^{eI}) T(\xi^{eI}) n_i^s(\xi^{eI}) \right] = 0, \quad \xi^{eI} \in \Gamma_I, \quad (27)$$

where  $N^I$  is the number of elements, including the interface node  $I$  under consideration,  $S^{eI}$  is the number of surfaces of element  $e$  associated with the interface node  $I$  (the definition of surfaces for 2D problems can be seen in Figure 5),  $\xi^{eI}$  is the intrinsic coordinate of element  $e$  at interface node  $I$ ,  $n_j^s$  is the outward normal to the surface  $s$ ,  $\Gamma_I$  represents the interface between elements, and  $t_i^s$  is the traction on the surface  $s$ . Figure 7 shows a 2D case for the interface node  $\xi^I$  shared by 4 elements' corners with 8 surfaces symbolized using  $\mathbf{n}_{(e)}^s$ , where  $\mathbf{n}_{(e)}^s$  represents  $\mathbf{n}^s(\xi^{eI})$ , whereas Figure 8 is the case for interface node  $\xi^I$  shared by 2 elements' edges with 2 surfaces symbolized using  $\mathbf{n}_{(1)}^1$  and  $\mathbf{n}_{(2)}^3$ , respectively.



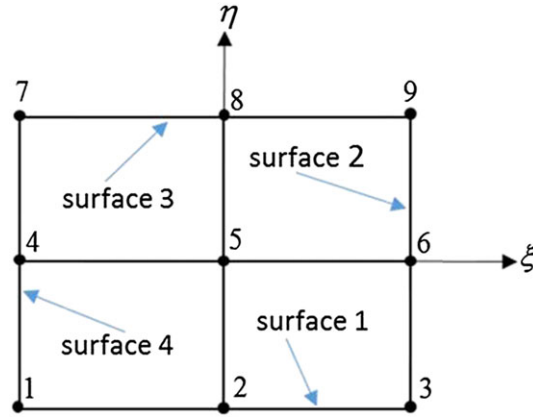


**FIGURE 5** Four surfaces defined over the 2D 9-node element

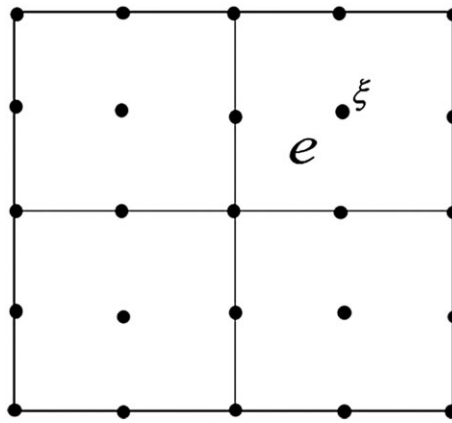


**FIGURE 6** Internal node  $\xi$  inside element  $e$

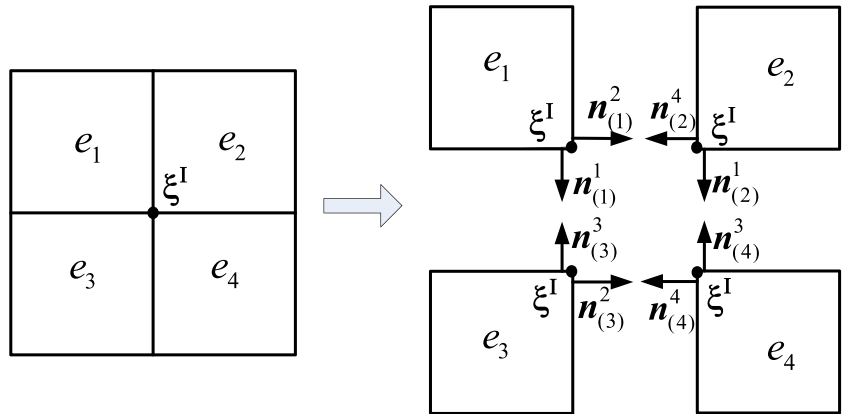


**FIGURE 7** Elemental surfaces related to interface node  $\xi^I$  shared by 4 elements' corners

### 4.3 | Setting up equations for outer boundary nodes based on traction equilibrium conditions

For a node located on the outer boundary of the problem, the node may associated with a part of interfaces and a part of outer surfaces. Therefore, the traction equilibrium condition on such a node can be express as

$$\sum_{e=1}^{N^b} \sum_{s=1}^{S^{eb}} t_i^s(\xi^{eb}) = \sum_{e=1}^{N^b} \sum_{l=1}^{S^{el}} t_i^l(\xi^{eb}) + \sum_{e=1}^{N^b} \sum_{s=1}^{S^{eo}} \bar{t}_i^s(\xi^{eb}) = \sum_{e=1}^{N^b} \sum_{s=1}^{S^{eo}} \bar{t}_i^s(\xi^{eb}), \quad (28)$$

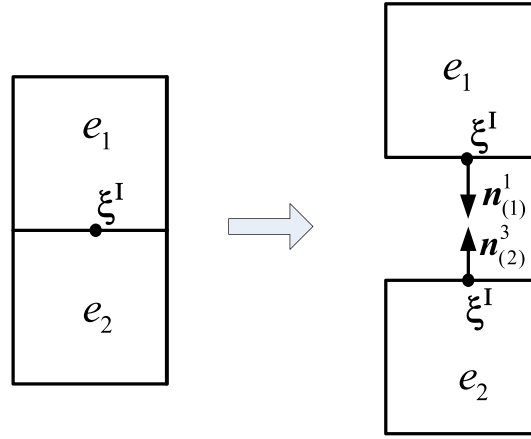


**FIGURE 8** Elemental surfaces related to interface node  $\xi^I$  shared by 2 elements' edges

where  $N^b$  is the number of elements, including the boundary node  $b$  under consideration,  $S^{eb}$  is the total number of surfaces of element  $e$  associated with the boundary node  $b$ ,  $S^{eI}$  and  $S^{eo}$  are the numbers of interfaces and outer surfaces, respectively,  $\xi^{eb}$  is the intrinsic coordinate of element  $e$  at the boundary node  $b$ ,  $t_i^I$  is the traction on the interface  $I$ , and  $\bar{t}_i^s$  is the external traction on the outer surface  $s$ . In the above equation, the traction equilibrium condition  $\sum_{e=1}^{N^b} \sum_{I=1}^{S^{eI}} t_i^I(\xi^{eb}) = 0$  has been used on the interfaces.

As an example, Figure 9 shows a 2D case for the boundary node  $\xi^b$  shared by 2 elements, in which  $\bar{t}_{(1)}^3$  and  $\bar{t}_{(2)}^3$  representing  $\bar{t}^3(\xi^{1b})$  and  $\bar{t}^3(\xi^{2b})$  are the external tractions on the third surfaces of the elements 1 and 2, respectively, whereas  $t_{(1)}^2$  and  $t_{(2)}^4$  are the tractions over 2 interfaces (the second interface of element 1 and the fourth interface of element 2, respectively), with  $t_{(1)}^2 + t_{(2)}^4 = 0$ . The used surfaces are defined in Figure 5.

Thus, substituting Equation 13 into Equation 7b and the results into Equation 28, it follows that

$$\sum_{e=1}^{N^b} \sum_{s=1}^{S^{eb}} \left[ D_{ijkl}(\xi^{eb}) n_j^s(\xi^{eb}) \frac{\partial N_\alpha(\xi^{eb})}{\partial x_l} u_k^\alpha - \tilde{k}(\xi^{eb}) T(\xi^{eb}) n_i^s(\xi^{eb}) \right] = \sum_{e=1}^{N^b} \sum_{s=1}^{S^{eo}} \bar{t}_i^s(\xi^{eb}), \quad \xi^{eb} \in \Gamma_t \quad (29)$$

It is noted that the assembling scheme of the system of equations described in the above equations can simulate the traction discontinuity across different elements at a same outer surface node. In other words, referencing Figure 9, the value of traction  $\bar{t}$  at the same node  $\xi^b$  can be different over the outer surfaces of elements  $e_1$  and  $e_2$  as split in the right figures in Figure 9, provided we specify different values for  $\bar{t}^3(\xi^{1b})$  and  $\bar{t}^3(\xi^{2b})$  when using Equation 29. The simulation of the traction discontinuity is a very challenging issue in BEM.<sup>50</sup> However, in EDM, it can be easily solved. It is noted that the boundary node  $\xi^b$  demonstrated in Figure 9 is an edge node. The same results and conclusions can be applied to a corner boundary node.

#### 4.4 | Forming the final system of equations

Collocating Equation 26 at internal nodes of elements and Equation 27 at interface nodes between elements, each of these nodes can generate an equation involving nodal values of displacement over all nodes of elements, including the considered node. Moreover, collocating Equation 29 at all outer boundary nodes, each of them can generate an equation involving nodal

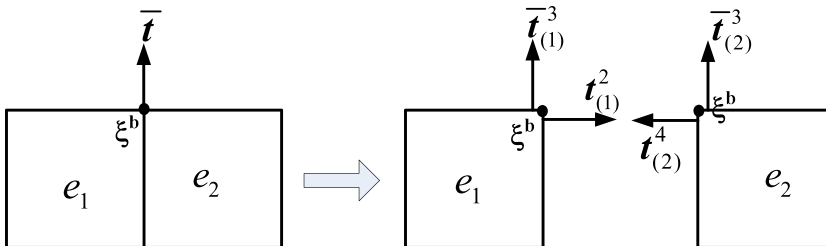


**FIGURE 9** Elemental surfaces associated with outer boundary node  $\xi^b$

displacements and tractions. Defining a global nodal vector of displacement, numbered in the global nodal sequence, each of the elemental nodes  $\alpha$  in Equations 26–29 corresponds to a position in the global nodal vector. For interface nodes shared by a number of elements, the displacement continuous condition,  $u_i^{(I)} = u_i^{(II)}$ , is used, with  $u_i^{(I)}$  and  $u_i^{(II)}$  being the displacements over the adjacent elements  $I$  and  $II$ , respectively, and they occupy the same position in the global displacement vector.

The unknowns in the final system of equations are numbered in the global nodal sequence. At each outer boundary node, either the displacement or the traction is specified. Thus, multiplying the specified values of displacement and traction in Equations 26–29 with corresponding coefficients, a known vector  $\mathbf{b}$  can be formed, and it is moved to the right-hand side of the system of equations. The remaining terms in Equations 26–29 associated with unknown displacements and unknown tractions are put on the left-hand side of the system of equations. At last, the final system of equations can be formed as follows:

$$\mathbf{A}\mathbf{x} = \mathbf{b}, \quad (30)$$

where  $\mathbf{x}$  is a vector containing unknown displacement or unknown traction of each node. By solving Equation 30 for vector  $\mathbf{x}$ , we can obtain all unknowns of the problem. It is noted that if the total number of all nodes used to discretize the problem is  $N$ , then the size of the coefficient matrix  $\mathbf{A}$  in Equation 30 is  $2N \times 2N$  for 2D problems and  $3N \times 3N$  for 3D problems. Because each equation in Equation 30 is only related to the nodes of elements associated with the node collocated to this equation, the matrix  $\mathbf{A}$  is sparse. This feature is in favor of applying a robust sparse matrix equation solver to solve Equation 30.

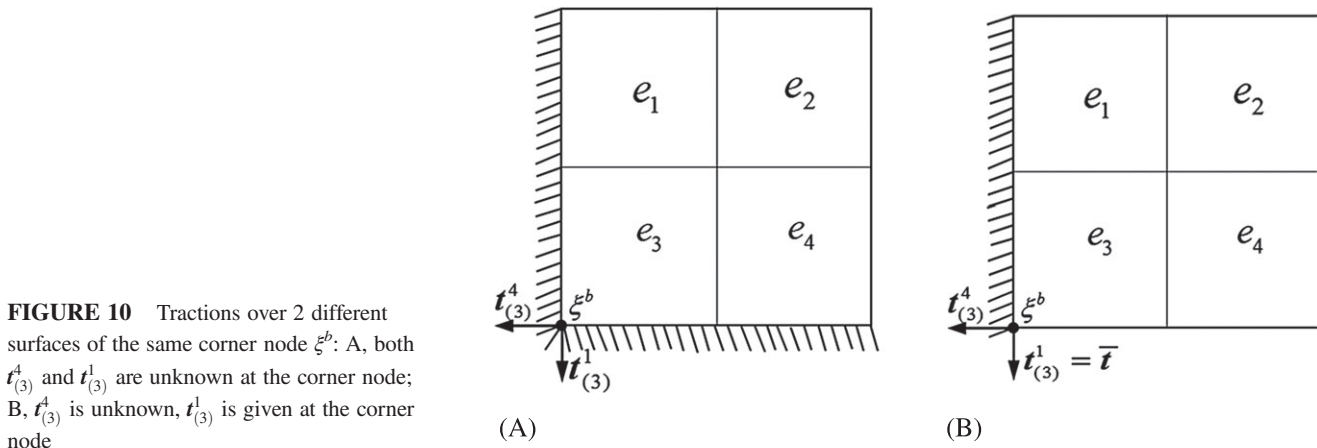
It also needs to be pointed out that, at a corner node (see Figure 10), if the displacement is specified, the number of unknown tractions in 1 direction may exceed 1 (the  $\mathbf{t}_{(3)}^4$  and  $\mathbf{t}_{(3)}^1$  in Figure 10A). In this case, in terms of Equation 29, the solved unknown for this node is the sum of these tractions (being  $\mathbf{t}_{(3)}^4 + \mathbf{t}_{(3)}^1$  in Figure 10A). If desired, Equation 7B can be used to compute the tractions  $\mathbf{t}_{(3)}^4$  and  $\mathbf{t}_{(3)}^1$  distributed on the corresponding surfaces by using the solved all nodal displacements. On the other hand, although the tractions at a corner node is discontinuous over different elemental surfaces (see Figure 10), if only 1 traction component is unknown in 1 direction (see Figure 10B), the solved unknown from Equation 30 is the true value of the traction component exactly on the unknown traction surface because all other known tractions have been incorporated into the vector  $\mathbf{b}$  and moved to the right-hand side of the system of Equation 30.

#### 4.5 | Evaluation of stresses

After all displacements at boundary and internal nodes are solved from Equation 30, the stresses defined in Equation 2 can be easily calculated using the following expression:

$$\sigma_{ij}(\xi^n) = D_{ijkl}(\xi^n) \frac{\partial N_\alpha(\xi^n)}{\partial x_l} u_k^\alpha - \tilde{k}(\xi^n) T(\xi^n) \delta_{ij}, \quad (31)$$

where  $\xi^n$  is the nodal intrinsic coordinate of the element, including the node to be calculated. It is noted that a node usually is shared by a number of elements. Therefore, Equation 31 is applied to all elements associated with the node under consideration, and the final value of the stress should take the average of all the elemental results.



## 5 | NUMERICAL EXAMPLES

To verify the correctness and to demonstrate the potential of the proposed method, 5 numerical examples are given.

### 5.1 | Example 1—patch test for a 2D square

To examine the dependence of the computational results on the number and quality of used elements, a square subjected to uniform extension displacements is analyzed. The geometry, boundary conditions, and material properties are shown in Figure 11. Pure elasticity analysis is performed without thermal load, and the plane strain problem is considered in this test. The exact displacement field is given by

$$\begin{cases} u(x, y) = x \\ v(x, y) = 2y \end{cases}$$

To investigate the convergence rate of the EDM, the 2D square is further meshed with more fine-scale grids. Some of the mesh grids with 16-node elements are shown in Figure 12.

The  $L_2$  error is used to examine the accuracy variation of the proposed method, which is defined as  $L_2 = \sqrt{(\mathbf{u} - \bar{\mathbf{u}}) \cdot (\mathbf{u} - \bar{\mathbf{u}})} / n$ , where  $\mathbf{u}$  and  $\bar{\mathbf{u}}$  are the computed displacement vector and analytical solution vector at all nodes, respectively with  $n$  being the rank of vector  $\mathbf{u}$ . Table 1 lists the  $L_2$  values for the 4 different meshes, and Figure 13 gives the variation of  $L_2$  versus the number of elements, which shows the varying trend of the  $L_2$  error. From Table 1, it can be seen that the  $L_2$  error of the computed displacements decreases as the numbers of elements and nodes increasing. This means that the proposed method can well pass the patch test.

### 5.2 | Example 2—a 2D beam subjected to a quadratic thermal loading

The second example is a 2D beam subjected to a quadratic thermal loading, which was analyzed using BEM<sup>17</sup> under plane strain condition. The beam with dimensions of  $L \times H$  (here  $L = 2$ ,  $H = 1$ ) is supported in roller conditions on 3 sides (see Figure 14) such that the uniaxial deformation can be captured. The temperature is assumed to be distributed as follows:

$$T(y) = c_2 y^2 + c_1 y, \quad c_2 = 40, \quad c_1 = -60.$$

The analytical solution to this problem can be derived as<sup>17</sup>

$$u_y(y) = \frac{1+\nu}{1-\nu} k \left\{ \frac{1}{3} c_2 [y^3 + (H/2)^3] + \frac{1}{2} c_1 [y^2 - (H/2)^2] \right\}, \quad \sigma_{xx} = -\frac{E}{1-\nu} k T.$$

The beam is analyzed using 2 different meshes of 9-node and 25-node Lagrange elements as shown in Figures 15A and 15B. In the 9-node mesh, there are totally 128 elements and 561 nodes, and in the 25-node one, the number of nodes is the same but the number of elements becomes 32. To examine the stability of the computational results on the element quality, 2 highly distorted

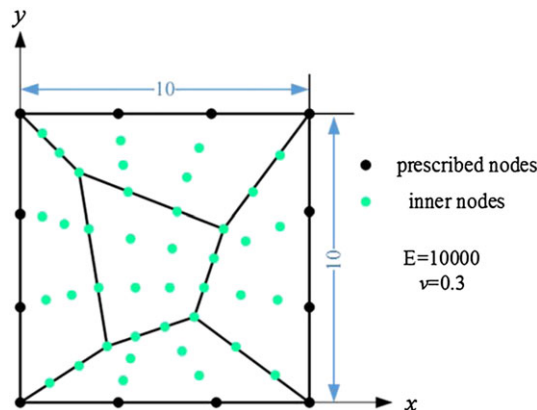


**FIGURE 11** Boundary conditions and materials for the patch test

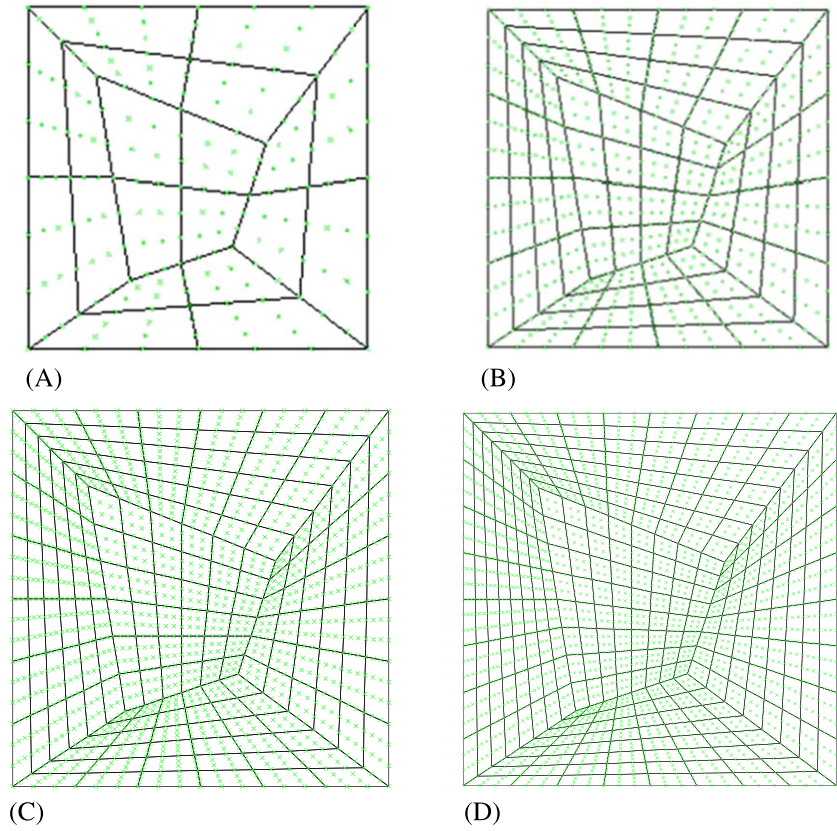


**FIGURE 12** The 2D square: domain discretized with A, 20 elements with 193 nodes, B 80 elements with 745 nodes, C 180 element with 1657 nodes, and D 320 element with 2929

**TABLE 1**  $L_2$  error of computed displacements for different meshes

Number of elements	5	20	45	80	180	320
Number of nodes	52	193	424	745	1657	2929
$L_2$ error	3.686E-9	1.897E-9	1.347E-9	1.019E-9	6.920E-10	5.210E-10

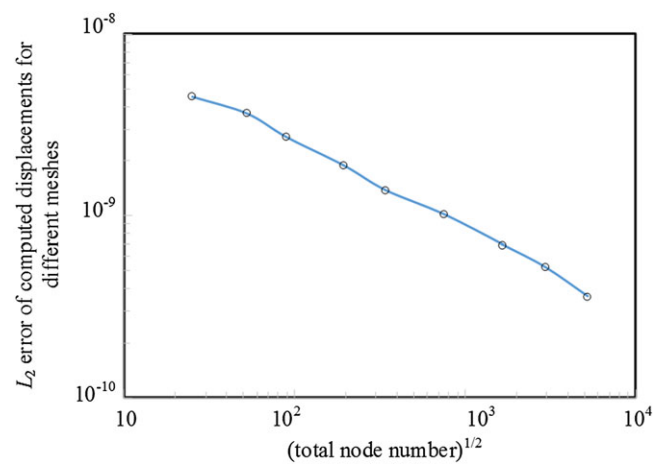


**FIGURE 13** Varying trend of the  $L_2$  error

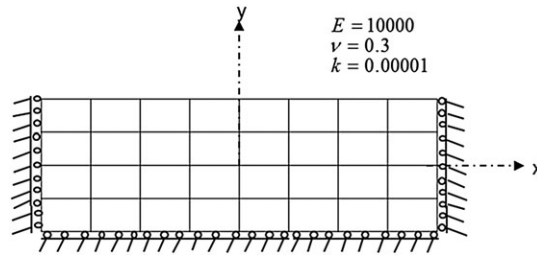


**FIGURE 14** BEM model of a beam subjected to a thermal loading

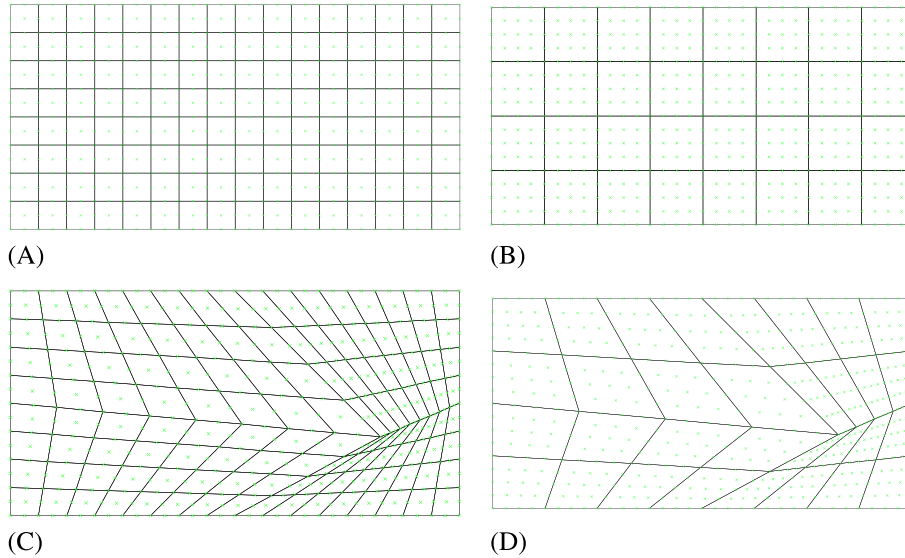


**FIGURE 15** Computational meshes used in the beam computation. A, Regular mesh of 9-node element; B, regular mesh of 25-node element; C, distorted mesh of 9-node element; D, distorted mesh of 25-node element

meshes for the 2 cases are also used as shown in Figures 15C and 15D. The computed displacements and stresses along the middle vertical line are listed in Tables 2–5 and plotted in Figures 16–19.

From Tables 2–5 and Figures 16–19, it can be seen that the analytical and numerical results are in good agreement. Even for distorted meshes, the results are still acceptable. This indicates that the proposed method is correct and the results have a good stability.

### 5.3 | Example 3: a thick plate subjected to a bending load

The third example is concerned with a 3D thick plate with the Young's modulus of  $E = 10^5$  MPa and Poisson ratio of  $\nu = 0.3$  under a uniformly distributed bending load  $f = 10$  MPa on the top surface. The dimensions of the plate are shown in Figure 20. In the computation using the current method EDM, the plate is discretized into 7200 27-node Lagrange elements with 63,257 nodes (see Figure 21). To validate the correctness of EDM, the problem is also computed using the FEM software ANSYS with a finer model of 25,000 Solid186 elements and 110,721 nodes. Figure 22 gives the distribution of the computed displacements  $u_z$  and  $u_x$  along the middle line of the top surface of the plate, whereas Figure 23 is a plot of the computed von Mises stresses<sup>50</sup> using the 2 methods.

From Figure 22, it can be seen that the computed displacements using current EDM are very close to the results using ANSYS. However, Figure 23 shows that the stresses computed using the 2 methods have a big discrepancy at the clamped end (at  $x = 0$ ) of the plate. This may be caused by the different ways to compute stresses in EDM and FEM. In EDM, the stresses are computed based on Equation 31 exactly at nodes, while in FEM, the stresses are computed at Gauss points

**TABLE 2** Computed displacement  $u_y$  ( $\times 10^{-5}$ ) based on regular mesh

y	9-node mesh	25-node mesh	Analytical
-0.375	7.904464	7.8600290	7.883190
-0.250	13.197321	13.116178	13.154760
-0.125	16.172232	16.061980	16.104910
0.00	17.115890	16.970340	17.023810
0.125	16.317322	16.144325	16.201640
0.250	14.067857	13.867412	13.928570
0.375	10.655350	10.418169	10.494790
0.500	6.3723215	6.0906434	6.1904800

**TABLE 3** Computed stress  $\sigma_{xx}$  based on regular mesh

y	9-node mesh	25-node mesh	Analytical
-0.375	-4.014286	-4.024975	-4.017860
-0.250	-2.500000	-2.499980	-2.500000
-0.125	-1.161429	-1.167126	-1.160710
0.00	-1.243450E-14	1.403600E-5	0.000000
0.125	0.982857	0.980725	0.982140
0.250	1.785714	1.785722	1.785710
0.375	2.414285	2.403576	2.410710

**TABLE 4** Computed displacement  $u_y$  ( $\times 10^{-5}$ ) based on distorted mesh

y	9-node mesh	25-node mesh	Analytical
-0.325	10.287771	10.268630	10.288960
-0.150	15.721742	15.693840	15.686670
-0.113	16.332802	16.303424	16.283420
0.194	15.215931	15.143327	15.112450
0.500	6.394046	6.108750	6.190476

**TABLE 5** Computed stress  $\sigma_{xx}$  based on distorted mesh

y	9-node mesh	25-node mesh	Analytical
-0.500	-5.7105674	-5.7145659	-5.71429
-0.325	-3.3789669	-3.3930307	-3.38929
-0.150	-1.4147519	-1.4338217	-1.41429
-0.113	-1.0337035	-1.0518641	-1.03661
0.194	1.4389297	1.4557955	1.446205
0.500	2.8552599	2.848482	2.857143

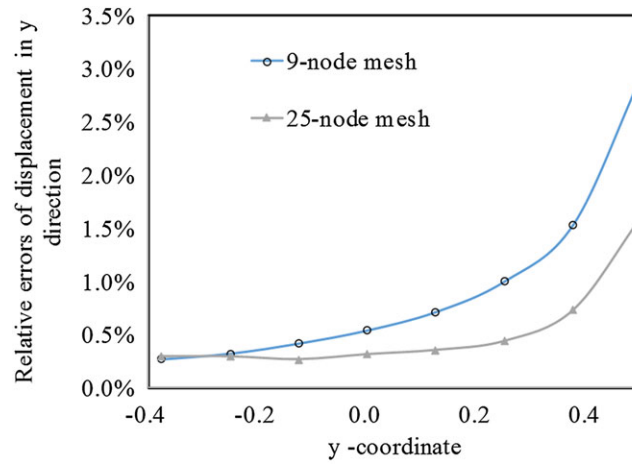


**FIGURE 16** Relative errors of the computed displacement  $u_y$  based on regular mesh

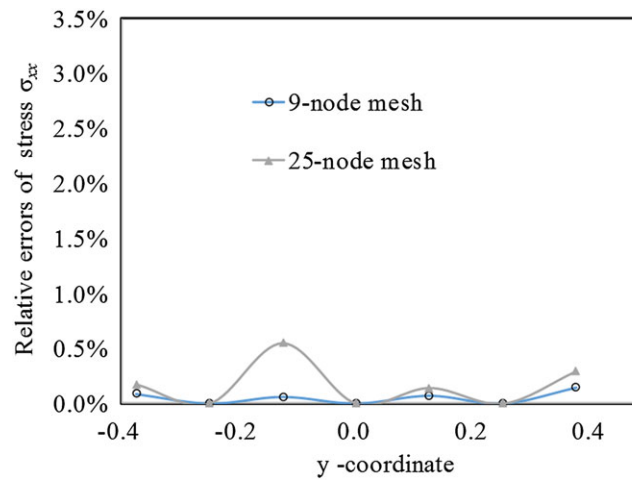


**FIGURE 17** Relative errors of the computed stress  $\sigma_{xx}$  based on regular mesh

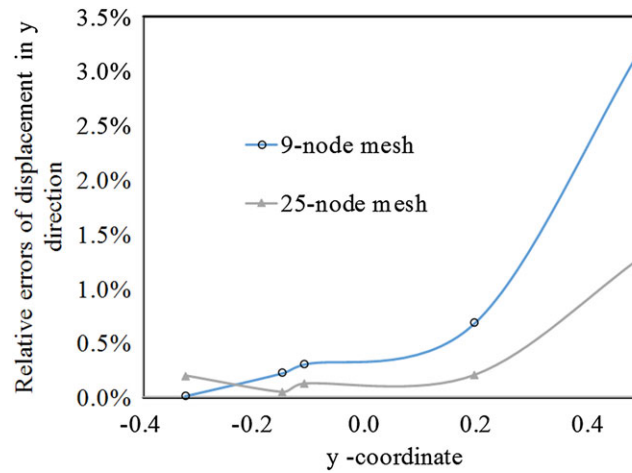


**FIGURE 18** Relative errors of the computed displacement  $u_y$  based on distorted mesh



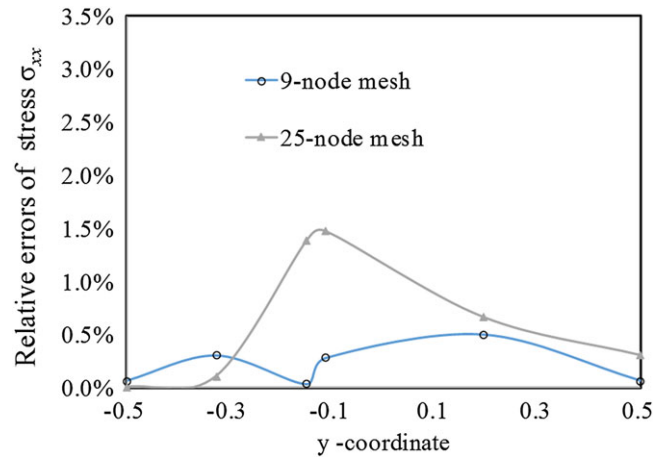


**FIGURE 19** Relative errors of the computed stress  $\sigma_{xx}$  based on distorted mesh

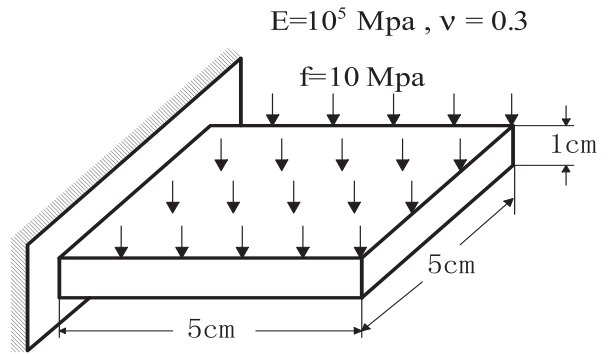


**FIGURE 20** A thick plate under a bending load

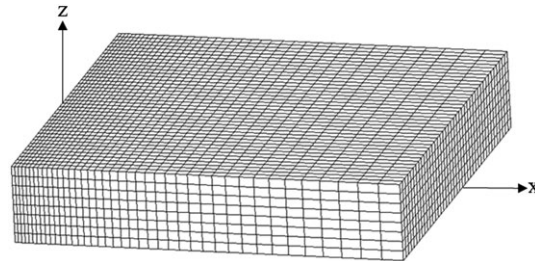


**FIGURE 21** EDM mesh of 27-node elements

within an element and nodal values are extrapolated through the values of Gauss points. Figure 23 also shows that, at the clamped end, the value of EDM is sharper than that of FEM. This indicates that EDM can reflect the stress concentration phenomenon better than FEM.

#### 5.4 | Example 4: thermoelastic analysis of the connector of a circular combustor

The fourth example is on the thermoelasticity analysis of the connector of a circular combustor of an aero-engine, which is aimed to show the application potential of EDM to solve practical engineering problems. The boundary conditions of the connector are shown in Figure 24. The inner diameter of the combustor is 7 cm, and the thickness of the combustor wall is 0.45 cm. The inner surface of the combustor is specified with a temperature of  $T_w = 1000K$  and a uniformly distributed pressure of

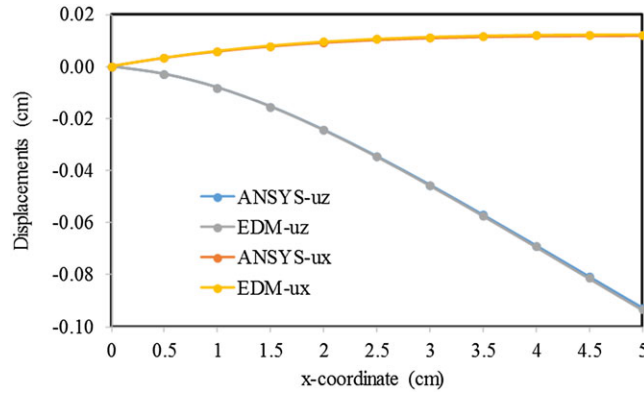


**FIGURE 22** Displacements  $u_z$  and  $u_x$  computed using ANSYS and EDM

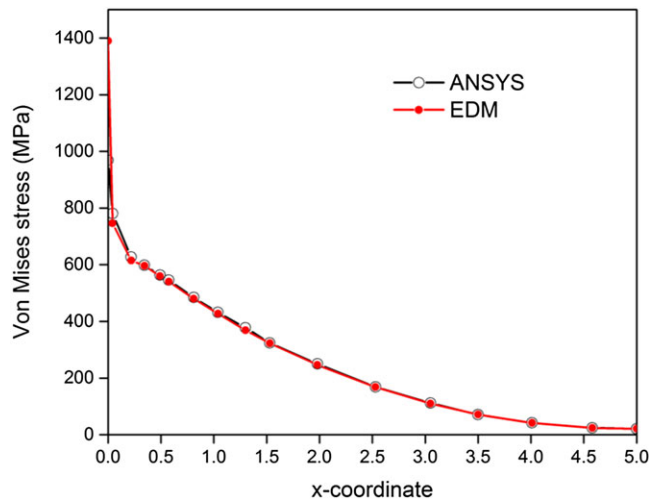


**FIGURE 23** von Mises stresses computed using ANSYS and EDM

2 MPa, whereas the outer surfaces of the combustor and the connector are exposed in the air with an environment of  $T_\infty = 300K$  and a pressure of 0.2 MPa. The 2 ends of the combustor are thermally insulated, and for mechanical loads, the left end is roller supported and the right end is traction free. The heat transfer coefficient between the air and the outer boundary of the combustor is  $h = 100 \text{ W/m}^2 \text{ K}$ , and the material properties are listed in Table 6.

Because of symmetry in the geometry about the axis of the combustor, only a quarter of the connector is analyzed. The whole connector is discretized into 21,400 27-node brick elements with total of 192,405 nodes, as shown in Figure 25. For comparison, the problem is also computed using the standard FEM software ANSYS with a very fine mesh.

First, the temperature field is computed using EDM based on the formulation described by Gao<sup>49</sup> for the heat conduction, and then the temperature field as input data is used in the thermoelasticity analysis. Figure 26 is the contour plot of the computed temperature field using EDM. Figures 27 and 28 show the temperature variation along lines AB and CD marked in Figure 26B and GH marked in Figure 25, whereas Figures 29 and 30 are the plot of displacements along these lines.

From Figures 27–30, it can be seen that the computed temperatures and displacements using the current method EDM are in excellent agreement with that using the commercial FEM software ANSYS. The maximum relative error between the 2 methods is within 1%. This indicates that the present method is correct and can be used to solve complicated engineering problems. The total computational time spending on this problem is 110 seconds in the temperature computation and 542 seconds in the thermoelasticity computation on a ThinkPad Laptop computer with CPU of 2.6GHz. These computational times show that high computational efficiency of the proposed method can be achieved. This is attributed to the fact that no integrations are required and a highly sparse system can be resulted in EDM.

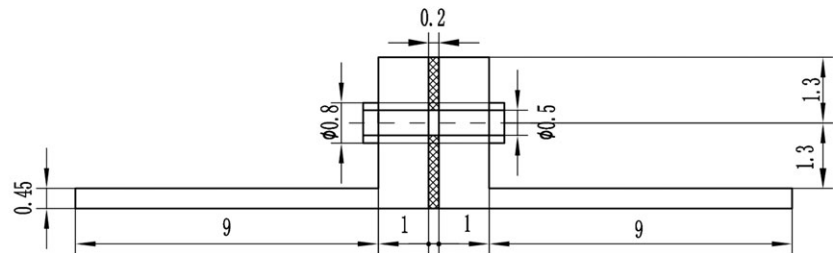
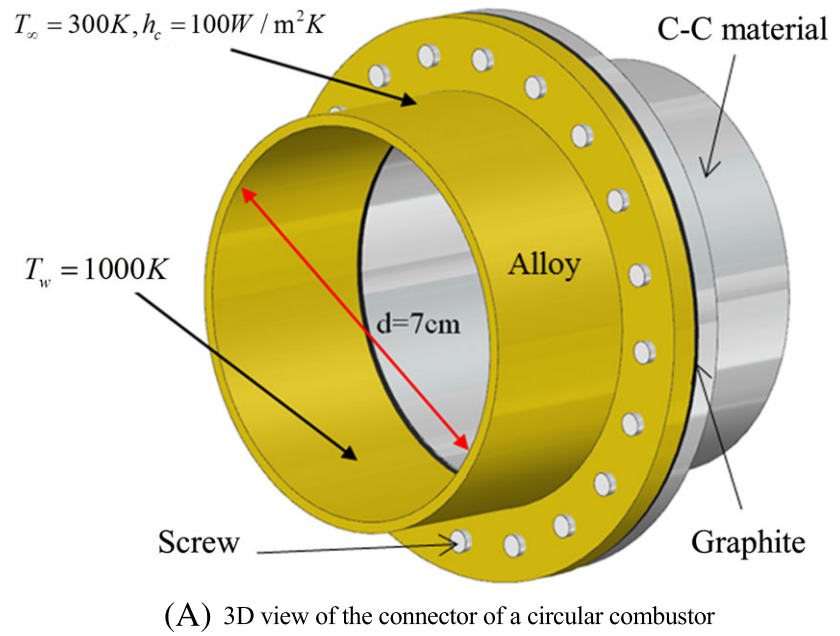


**FIGURE 24** The connector of a circular combustor: A, 3D view; B, cross section

**TABLE 6** Mechanical and thermal material properties

	Young's modulus, $E$ (GPa)	Poisson ratio, $\nu$	Coefficient of expansion, $k$ ( $\times 10^{-6}$ )	Heat conductivity, $\lambda$ (W/mK)
Alloy	179.5	0.327	14.	15
C-C material	90.	0.2	5.72	150
Graphite	1.38	0.05	28.8	300

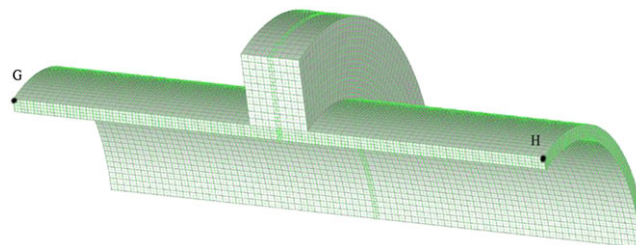
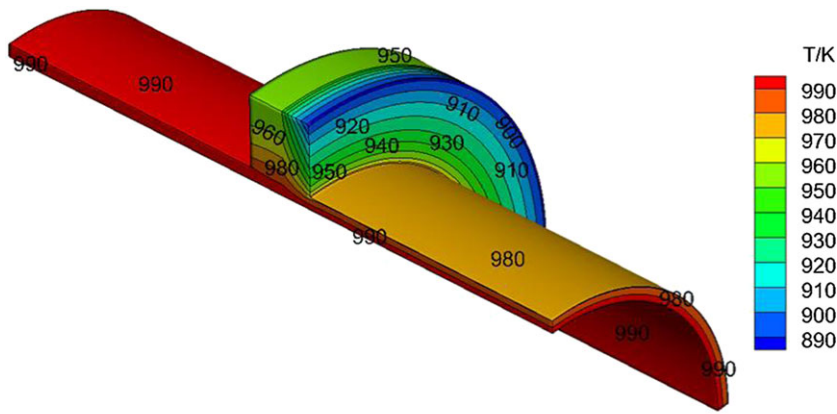
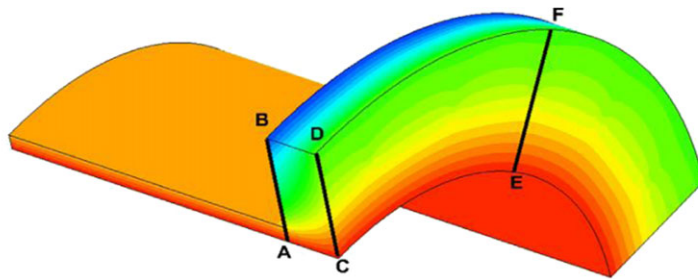


**FIGURE 25** The computational mesh used in EDM computation



(A) Overall view of the temperature distribution



(B) Temperature over the alloy part

**FIGURE 26** Contour plot of the temperature field: A, overall view; B, alloy part

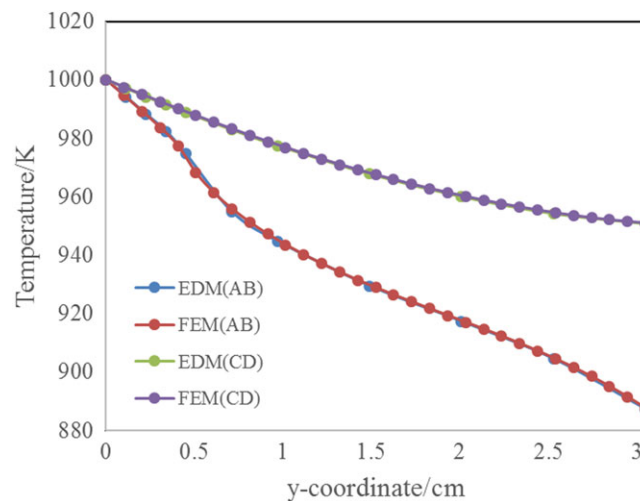


**FIGURE 27** Temperature distribution along lines AB and CD marked in Figure 26B

## 5.5 | Example 5: thick-walled cylinder under internal pressure

In order to verify the advantages of EDM over TCM, a thick cylinder with an inner and outer diameters of 200 and 400 units subjected to an internal pressure of  $P = 0.4$  MPa is examined under plane stress conditions as depicted in Figure 31.

Because of symmetry, a quarter of the cylinder is analyzed. The material properties are elastic modules  $E = 2.1 \times 10^6$  and Poisson's ratio  $\nu = 0.3$ . The model is analyzed using 9-node Lagrange elements as shown in Figure 32.

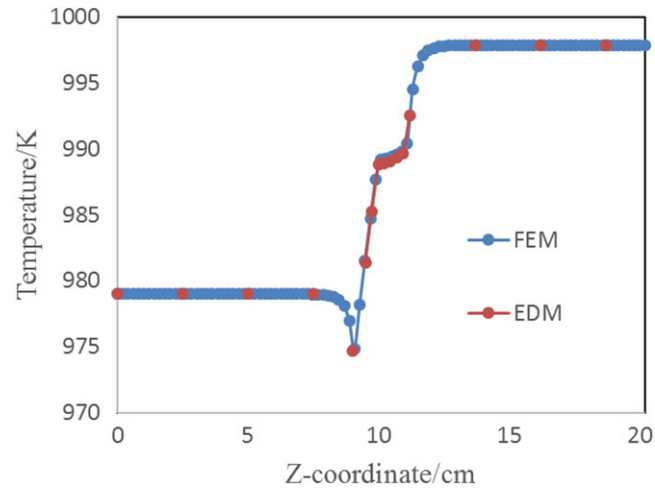


**FIGURE 28** Temperature distribution along the longitudinal line GH marked in Figure 25

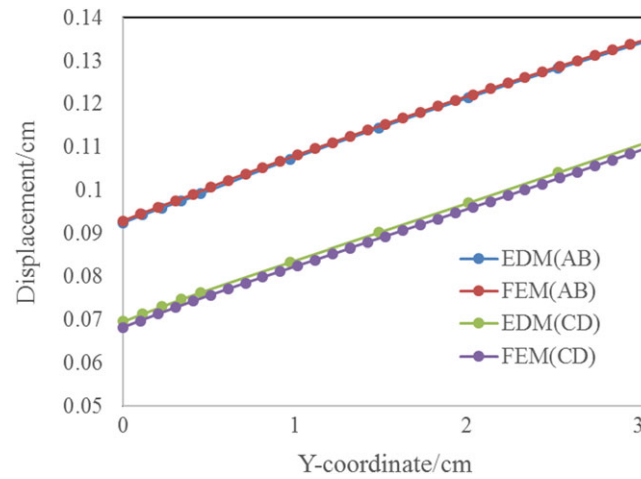


**FIGURE 29** Displacement  $u_y$  along lines AB and CD marked in Figure 26B

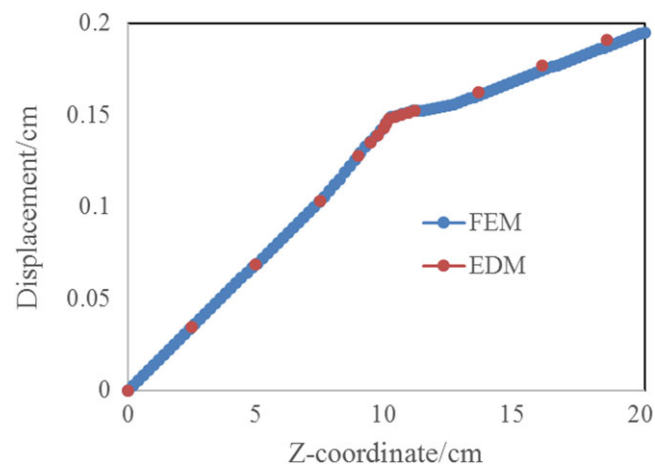


**FIGURE 30** Displacement  $u_z$  along the longitudinal line GH marked in Figure 25

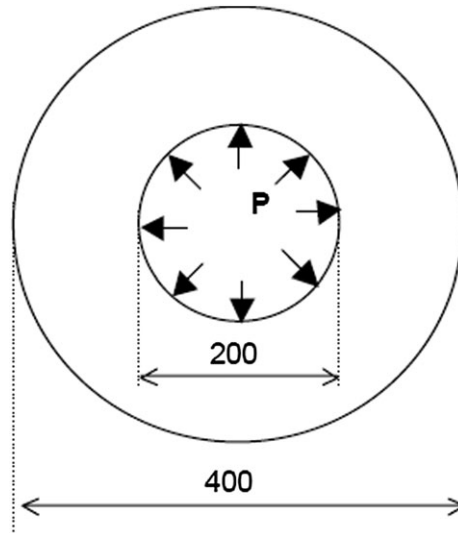


**FIGURE 31** Thick cylinder under internal pressure

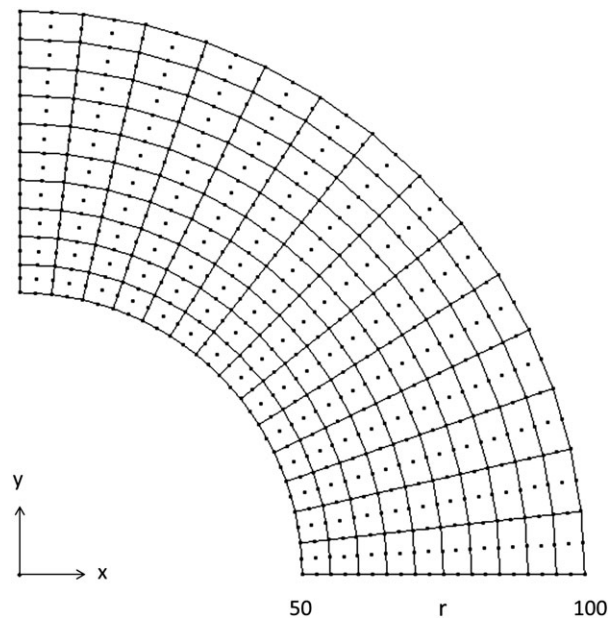


**FIGURE 32** The computational mesh used in EDM

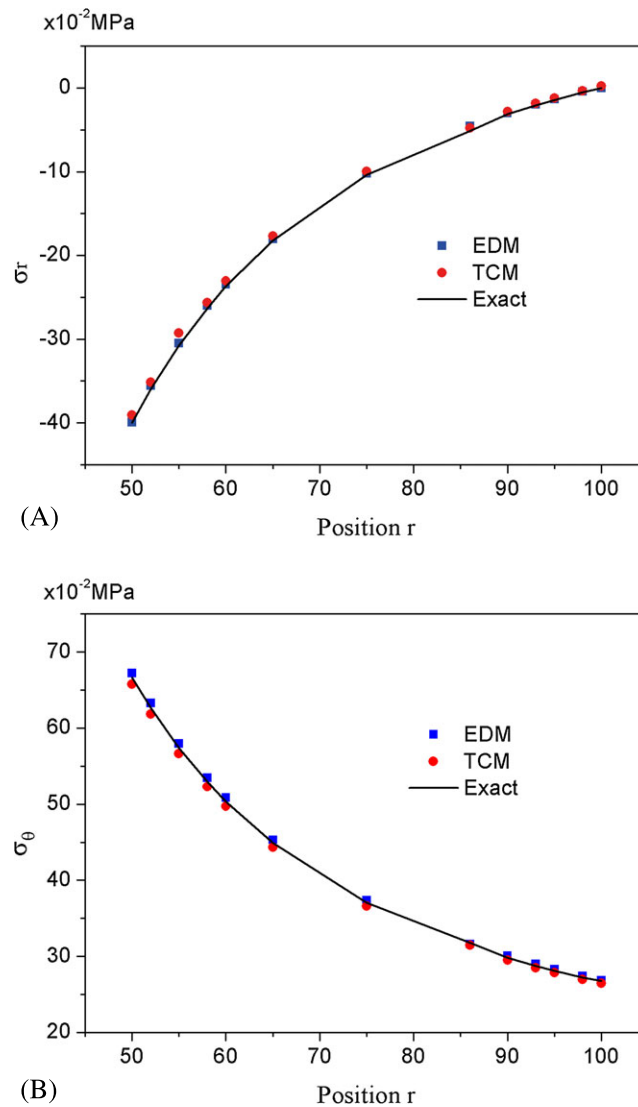
**TABLE 7** Computed results compared with other results  $\times 10^{-2}$  MPa

Position r	EDM results		TCM results <sup>51</sup>		Exact solution	
	$\sigma_r$	$\sigma_\theta$	$\sigma_r$	$\sigma_\theta$	$\sigma_r$	$\sigma_\theta$
50	-39.94	67.209	-39.09	65.76	-40	66.67
52	-35.561	63.28	-35.14	61.8	-35.98	62.64
55	-30.496	57.955	-29.29	56.66	-30.74	57.41
58	-26.023	53.484	-25.63	52.29	-26.3	52.97
60	-23.445	50.857	-23.07	49.74	-23.7	50.37

(Continues)

**TABLE 7** (Continued)

Position $r$	EDM results		TCM results <sup>51</sup>		Exact solution	
	$\sigma_r$	$\sigma_\theta$	$\sigma_r$	$\sigma_\theta$	$\sigma_r$	$\sigma_\theta$
65	-18.039	45.309	-17.69	44.35	-18.23	44.89
75	-10.226	37.371	-9.97	36.63	-10.37	37.04
86	-4.57	31.636	-4.81	31.47	-5.12	31.79
90	-3.013	30.051	-2.85	29.51	-3.13	29.79
93	-1.982	28.991	-1.82	28.49	-2.08	28.75
95	-1.344	28.341	-1.19	27.85	-1.44	28.11
98	-0.44	27.445	-0.32	26.98	-0.55	27.22
100	6.77E-03	26.859	0.22	26.44	0	26.76

**FIGURE 33** Comparison of stresses: A  $\sigma_r$  B  $\sigma_\theta$

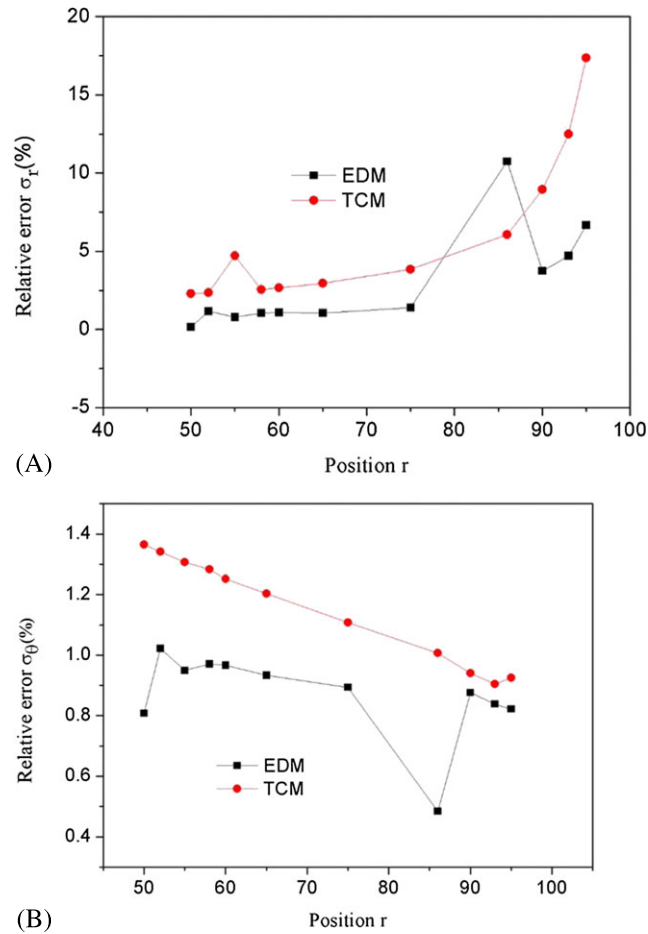


**FIGURE 34** The relative error to the exact solution: A  $\sigma_r$  B  $\sigma_\theta$

Table 7 gives the computed stresses for the problem and Figures 33 and 34 are the plot of the results. For comparison, results obtained using the TCM<sup>51</sup> and the exact solution are also provided. From Figures 33 and 34, it can be seen that the present EDM results are in very good agreement with the exact solution and more accurate than the TCM.

## 6 | CONCLUDING DISCUSSIONS

A new method, EDM, has been proposed for solving general second-order PDEs based on the use of Lagrange isoparametric elements. The following conclusions and discussions can be drawn:

1. The method is a strong-form technique and belongs to the categories of FEM, FBM, and the collocation method. However, it is easier to be coded than FEM and is able to generate smaller system and more accurate results than FBM and can obtain more stable solution than the collocation method.
2. Because EDM adopts the Lagrange isoparametric elements to discretize the geometry of the problem and represent physical variables, the specified boundary conditions can be directly imposed on the system of equations, more convenient than MFM.
3. The analytical expressions of computing spatial derivatives are only derived for the first- and second-order derivatives. If high-order differential equations will be solved using EDM, the relevant high-order derivatives can be generated by recursively using the first and second derivative expressions as done in FBM.
4. The system of equations established in this paper is formulated in terms of the primary physical variables, the displacements and tractions. It is exactly the same as that generated in BEM<sup>50</sup> for boundary nodes, and therefore, EDM can be directly combined with BEM to solve complicated problems.



5. The final system formed in the paper is not symmetric. Therefore, the existing equation solvers used in the traditional FEM may not be used to solve the system. However, as in FEM, the final system is sparse, such that some existing robust sparse equation solvers, such as the PARDISO\_UNSYM solver in the MKL library of the Intel Fortran, can be used to solve the system of equations for large-scale engineering problems.
6. The method presented in the paper is only about the spatial discretization. For time-dependent problems, we need also to handle the time derivatives, and for nonlinear problems, we need also to perform the iterative process to solve the system of equations. The techniques to handle these 2 types of problems are essentially the same as those used in the standard FEM, FVM, and MFM, which are already well developed and can be naturally extended to the methods proposed in this paper.

## ACKNOWLEDGMENTS

The support of this investigation by the National Natural Science Foundation of China under grant nos. 11672061, 11572075, and 11302040 is gratefully acknowledged.

## REFERENCES

1. Liu GR. An overview on meshfree methods: for computational solid mechanics. *Int J Comput Methods*. 2016;13(5): 1630001.
2. Zienkiewicz OC, Taylor RL. *The Finite Element Method*. London, UK: McGraw-Hill; 1989.
3. Hughes TJR. *The Finite Element Method: Linear Static and Dynamic Finite Element Analysis*. New Jersey, USA: Prentice-Hall; 1987.
4. Belytschko T, Liu WK, Moran B, Elkhodary K. *Nonlinear Finite Elements for Continua and Structures*. New York, USA: John Wiley & Sons; 2000.
5. Liu GR, Quek SS. *The Finite Element Method: A Practical Course*. 2nd ed. Oxford, UK: Butterworth-Heinemann; 2013.
6. Bochev PB, Gunzburger MD. *Least-Squares Finite Element Methods*. New York, USA: Springer; 2009.
7. Lv J, Sheng GY, Gao XW, Zhang HW. Numerical integration approach based on radial integration method for general 3D polyhedral finite elements. *Int J Comput Methods*. 2015;12(5):1550026-1-21.
8. Schröder J, Viebahn N, Balzani D, Wriggers P. A novel mixed finite element for finite anisotropic elasticity; the SKA-element simplified kinematics for anisotropy. *Comput Methods Appl Mech Eng*. 2016;310:475-494.
9. Brebbia CA, Telles JC, Wrobel LC. *Boundary Element Techniques*. Berlin: Springer; 1984.
10. Banerjee PK. *Boundary Element Method*. New York, USA: McGraw-Hill; 1992.
11. Divo E, Kassab AJ. *Boundary Element Method for Heat Conduction: With Applications in Non-homogenous Media*. Southampton, UK: WIT press; 2003.
12. Sladeka V, Sladeka J, Tanakab M, Zhang C. Transient heat conduction in anisotropic and functionally graded media by local integral equations. *Eng Anal Bound Elem*. 2005;29(11):1047-1065.
13. Gao XW, Peng HF, Liu J. A boundary-domain integral equation method for solving convective heat transfer problems. *Int J Heat Mass Transfer*. 2013;63(3):183-190.
14. Gao XW, Feng WZ, Zheng BJ, Yang K. An interface integral equation method for solving general multi-medium mechanics problems. *Int J Numer Methods Eng*. 2016;107(8):696-720.
15. AL-Jawary MA, Wrobel LC. Radial integration boundary integral and integro-differential equation methods for two-dimensional heat conduction problems with variable coefficients. *Eng Anal Bound Elem*. 2012;36:685-695.
16. Liu YJ. *Fast Multipole Boundary Element Method - Theory and Applications in Engineering*. Cambridge, UK: Cambridge University Press; 2009.
17. Gao XW. Boundary element analysis in thermoelasticity with and without internal cells. *Int J Numer Methods Eng*. 2003;57(7):975-990.
18. Gao XW. A meshless BEM for isotropic heat conduction problems with heat generation and spatially varying conductivity. *Int J Numer Methods Eng*. 2006;66(9):1411-1431.
19. Gao XW. An effective method for numerical evaluation of general 2D and 3D high-order singular boundary integrals. *Comput Methods Appl Mech Eng*. 2010;199(45-48):2856-2864.
20. Zhang JM, Tanaka M, Matsumoto T. A simplified approach for heat conduction analysis of CNT-based nano-composites. *Comput Methods Appl Mech Eng*. 2004;193(52):5597-5609.
21. Zhang JM, Qin XY, Han X, Li GY. A boundary face method for potential problems in three dimensions. *Int J Numer Methods Eng*. 2009;80(3):320-337.
22. Yang K, Feng WZ, Gao XW. A new approach for computing hyper-singular interface stresses in IIBEM for solving multi-medium elasticity problems. *Comput Methods Appl Mech Eng*. 2015;287(2):54-68.

23. Tao WQ, He YL, Wang QW, Qu ZG, Song FQ. A unified analysis on enhancing single phase convective heat transfer with field synergy principle. *In J Heat Mass Transfer*. 2002;45(24):4871-4879.
24. Li J, Peterson GP, Cheng P. Dynamic characteristics of transient boiling on a square platinum microheater under millisecond pulsed heating. *Int J Heat Mass Transfer*. 2008;51(1):273-282.
25. Tao YB, He YL, Liu YK, Tao WQ. Performance optimization of two-stage latent heat storage unit based on entransy theory. *Int J Heat Mass Transfer*. 2014;77(4):695-703.
26. Yang LH, Quan XJ, Cheng P, Cheng ZM. A free energy model and availability analysis for onset of condensation on rigid and liquid surfaces in moist air. *Int J Heat Mass Transfer*. 2014;78(7):460-467.
27. Gu YT, Liu GR. A meshfree weak-strong (MWS) form method for time dependent problems. *Comput Mech*. 2005;35(2):134-145.
28. Zhang X, Liu XH, Song KZ, Lu MW. Least-square collocation meshless method. *Int J Numer Methods Eng*. 2001;51(9):1089-1100.
29. Wang D, Wu J. An efficient nesting sub-domain gradient smoothing integration algorithm with quadratic exactness for Galerkin meshfree methods. *Comput Methods Appl Mech Eng*. 2016;298:485-519.
30. Wang D, Zhang H. A consistently coupled isogeometric-meshfree method. *Comput Methods Appl Mech Eng*. 2014;268:843-870.
31. Wen PH, Aliabadi MH. An improved meshless collocation method for elastostatic and elastodynamic problems. *Commun Numer Methods Eng*. 2008;24(8):635-651.
32. Zheng BJ, Gao XW, Yang K, Zhang C. A novel meshless local Petrov-Galerkin method for dynamic coupled thermoelasticity analysis under thermal and mechanical shock loading. *Eng Anal Bound Elem*. 2015;60:154-161.
33. Haq S, Hussain A, Uddin M. RBFs meshless method of lines for the numerical solution of time-dependent nonlinear coupled partial differential equations. *Appl Math*. 2011;2(4):414-423.
34. Khater AH, Temsah RS, Hassan MM. A chebyshev spectral collocation method for solving burgers' type equations. *J Comput Appl Math*. 2008;222(2):333-350.
35. Islam S, Haq S, Uddin M. A mesh free interpolation method for the numerical solution of the coupled nonlinear partial differential equations. *Eng Anal Bound Elem*. 2009;33(3):399-409.
36. Uddin M, Haq S, Islam S. Numerical solution of complex modified kortewegde vries equation by mesh-free collocation method. *Comput Math Appl*. 2009;58(3):566-578.
37. Jensen PS. Finite difference techniques for variable grids. *Comput Struct*. 1972;2(1-2):17-29.
38. Liszka T, Orkisz J. The finite difference method at arbitrary irregular grids and its application in applied mechanics. *Comput Struct*. 1980;11(1-2):83-95.
39. Liu GR, Zhang J, Li H, Lam KY, Kee BBT. Radial point interpolation based finite difference method for mechanics problems. *Int J Numer Methods Eng*. 2006;68(7):728-754.
40. Cui M, Duan WW, Gao XW. A new inverse analysis method based on a relaxation factor optimization technique for solving transient nonlinear inverse heat conduction problems. *Int J Heat Mass Transfer*. 2015;90:491-498.
41. Cui M, Yang K, Xu XL, Wang SD, Gao XW. A modified Levenberg-Marquardt algorithm for simultaneous estimation of multi-parameters of boundary heat flux by solving transient nonlinear inverse heat conduction problems. *Int J Heat Mass Transfer*. 2016;97:908-916.
42. Bishay PL, Sladek J, Sladek V, Gao XW. Analysis of elastic media with voids using a mixed-collocation finite-element method. *J Eng Mech*. 2016; (Online).
43. Dai W. A new accurate finite difference scheme for Neumann (insulated) boundary condition of heat conduction. *Int J Therm Sci*. 2010;49(3):571-579.
44. Han F, Dai W. New higher-order compact finite difference schemes for 1D heat conduction equations. *App Math Model*. 2013;37(16-17):7940-7952.
45. Yosaf A, Rehman SU, Ahmad F, Ullah MZ, Alshomrani AS. Eighth-order compact finite difference scheme for 1D heat conduction equation. *Adv Numer Anal*. 2016; 8376061.
46. Wen PH, Cao P, Korakianitis T. Finite block method in elasticity. *Eng Anal Bound Elem*. 2014;46:116-125.
47. Li M, Wen PH. Finite block method for transient heat conduction analysis in functionally graded media. *Int J Numer Methods Eng*. 2014;99(5):372-390.
48. Li M, Monjiza A, Xu YG, Wen PH. Finite block Petrov-Galerkin method in transient heat conduction. *Eng Anal Bound Elem*. 2015;60:106-114.
49. Gao XW. Element differential method (EDM) for solving heat conduction problems with varying conductivities and sources. *The 1st Asian Conference on Thermal Sciences*, Mach 26-30,2017, Jeju Island, Korea.
50. Gao XW, Davies TG. *Boundary Element Programming in Mechanics*. Cambridge, UK: Cambridge University Press; 2002.
51. Sun HC, Li XH, Zhang LZ. Virtual boundary element-collocation method for solving problems of elasticity. *Comput Struct Mech Appl*. 1991;8(1):15-23.

**How to cite this article:** Gao X-W, Li Z-Y, Yang K, et al. Element differential method and its application in thermal-mechanical problems. *Int J Numer Methods Eng*. 2017;1–27. <https://doi.org/10.1002/nme.5604>

## APPENDIX A: DERIVATIVES OF THE JACOBIAN INVERSE MATRIX FOR 3D PROBLEMS

**A1** | Used in Equation 23, for 3D problems, the following expressions can be obtained through a tedious derivation on Equations 21 and 22:

$$\frac{\partial[A]}{\partial\xi} = \begin{bmatrix} y_{\eta\xi}z_{\zeta} + y_{\eta}z_{\xi\xi} - y_{\xi\xi}z_{\eta} - y_{\xi}z_{\eta\xi} & y_{\xi\xi}z_{\eta} + y_{\xi}z_{\xi\xi} - y_{\xi\xi}z_{\xi} - y_{\xi}z_{\xi\xi} & y_{\xi\xi}z_{\eta} + y_{\xi}z_{\eta\xi} - y_{\eta\xi}z_{\xi} - y_{\eta}z_{\xi\xi} \\ x_{\xi\xi}z_{\eta} + x_{\xi}z_{\eta\xi} - x_{\eta\xi}z_{\xi} - x_{\eta}z_{\xi\xi} & x_{\xi\xi}z_{\xi} + x_{\xi}z_{\xi\xi} - x_{\xi\xi}z_{\xi} - x_{\xi}z_{\xi\xi} & x_{\eta\xi}z_{\xi} + x_{\eta}z_{\xi\xi} - x_{\xi\xi}z_{\eta} - x_{\xi}z_{\eta\xi} \\ x_{\eta\xi}y_{\xi} + x_{\eta}y_{\xi\xi} - x_{\xi\xi}y_{\eta} - x_{\xi}y_{\eta\xi} & x_{\xi\xi}y_{\xi} + x_{\xi}y_{\xi\xi} - x_{\xi\xi}y_{\xi} - x_{\xi}y_{\xi\xi} & x_{\xi\xi}y_{\eta} + x_{\xi}y_{\eta\xi} - x_{\eta\xi}y_{\xi} - x_{\eta}y_{\xi\xi} \end{bmatrix} \quad (A1)$$

$$\frac{\partial[A]}{\partial\eta} = \begin{bmatrix} y_{\eta\eta}z_{\xi} + y_{\eta}z_{\xi\eta} - y_{\xi\eta}z_{\eta} - y_{\xi}z_{\eta\eta} & y_{\xi\eta}z_{\xi} + y_{\xi}z_{\xi\eta} - y_{\xi\eta}z_{\xi} - y_{\xi}z_{\xi\eta} & y_{\xi\eta}z_{\eta} + y_{\xi}z_{\eta\eta} - y_{\eta\eta}z_{\xi} - y_{\eta}z_{\xi\eta} \\ x_{\xi\eta}z_{\eta} + x_{\xi}z_{\eta\eta} - x_{\eta\eta}z_{\xi} - x_{\eta}z_{\xi\eta} & x_{\xi\eta}z_{\xi} + x_{\xi}z_{\xi\eta} - x_{\xi\eta}z_{\xi} - x_{\xi}z_{\xi\eta} & x_{\eta\eta}z_{\xi} + x_{\eta}z_{\xi\eta} - x_{\xi\eta}z_{\eta} - x_{\xi}z_{\eta\eta} \\ x_{\eta\eta}y_{\xi} + x_{\eta}y_{\xi\eta} - x_{\xi\eta}y_{\eta} - x_{\xi}y_{\eta\eta} & x_{\xi\eta}y_{\xi} + x_{\xi}y_{\xi\eta} - x_{\xi\eta}y_{\xi} - x_{\xi}y_{\xi\eta} & x_{\xi\eta}y_{\eta} + x_{\xi}y_{\eta\eta} - x_{\eta\eta}y_{\xi} - x_{\eta}y_{\xi\eta} \end{bmatrix} \quad (A2)$$

$$\frac{\partial[A]}{\partial\zeta} = \begin{bmatrix} y_{\eta\xi}z_{\xi} + y_{\eta}z_{\xi\xi} - y_{\xi\xi}z_{\eta} - y_{\xi}z_{\eta\xi} & y_{\xi\xi}z_{\xi} + y_{\xi}z_{\xi\xi} - y_{\xi\xi}z_{\xi} - y_{\xi}z_{\xi\xi} & y_{\xi\xi}z_{\eta} + y_{\xi}z_{\eta\xi} - y_{\eta\xi}z_{\xi} - y_{\eta}z_{\xi\xi} \\ x_{\xi\xi}z_{\eta} + x_{\xi}z_{\eta\xi} - x_{\eta\xi}z_{\xi} - x_{\eta}z_{\xi\xi} & x_{\xi\xi}z_{\xi} + x_{\xi}z_{\xi\xi} - x_{\xi\xi}z_{\xi} - x_{\xi}z_{\xi\xi} & x_{\eta\xi}z_{\xi} + x_{\eta}z_{\xi\xi} - x_{\xi\xi}z_{\eta} - x_{\xi}z_{\eta\xi} \\ x_{\eta\xi}y_{\xi} + x_{\eta}y_{\xi\xi} - x_{\xi\xi}y_{\eta} - x_{\xi}y_{\eta\xi} & x_{\xi\xi}y_{\xi} + x_{\xi}y_{\xi\xi} - x_{\xi\xi}y_{\xi} - x_{\xi}y_{\xi\xi} & x_{\xi\xi}y_{\eta} + x_{\xi}y_{\eta\xi} - x_{\eta\xi}y_{\xi} - x_{\eta}y_{\xi\xi} \end{bmatrix} \quad (A3)$$

and

$$\begin{aligned} \frac{\partial|J|}{\partial\xi} = & x_{\xi\xi}y_{\eta}z_{\xi} + x_{\xi}y_{\eta\xi}z_{\xi} + x_{\xi}y_{\eta}z_{\xi\xi} - x_{\eta\xi}y_{\xi}z_{\xi} - x_{\eta}y_{\xi\xi}z_{\xi} - x_{\eta}y_{\xi}z_{\xi\xi} \\ & - x_{\xi\xi}y_{\xi}z_{\eta} - x_{\xi}y_{\xi\xi}z_{\eta} - x_{\xi\xi}y_{\xi}z_{\eta\xi} + x_{\xi\xi}y_{\xi}z_{\eta} + x_{\xi}y_{\xi\xi}z_{\eta} + x_{\xi}y_{\xi}z_{\eta\xi} \\ & + x_{\eta\xi}y_{\xi}z_{\xi} + x_{\eta}y_{\xi\xi}z_{\xi} + x_{\eta}y_{\xi}z_{\xi\xi} - x_{\xi\xi}y_{\eta}z_{\xi} - x_{\xi}y_{\eta\xi}z_{\xi} - x_{\xi}y_{\eta}z_{\xi\xi} \end{aligned} \quad (A4)$$

$$\begin{aligned} \frac{\partial|J|}{\partial\eta} = & x_{\xi\eta}y_{\eta}z_{\xi} + x_{\xi}y_{\eta\eta}z_{\xi} + x_{\xi}y_{\eta}z_{\xi\eta} - x_{\eta\eta}y_{\xi}z_{\xi} - x_{\eta}y_{\xi\eta}z_{\xi} - x_{\eta}y_{\xi}z_{\xi\eta} \\ & - x_{\xi\eta}y_{\xi}z_{\eta} - x_{\xi}y_{\xi\eta}z_{\eta} - x_{\xi\eta}y_{\xi}z_{\eta\xi} + x_{\xi\eta}y_{\xi}z_{\eta} + x_{\xi}y_{\xi\eta}z_{\eta} + x_{\xi}y_{\xi}z_{\eta\xi} \\ & + x_{\eta\eta}y_{\xi}z_{\xi} + x_{\eta}y_{\xi\eta}z_{\xi} + x_{\eta}y_{\xi}z_{\xi\eta} - x_{\xi\eta}y_{\eta}z_{\xi} - x_{\xi}y_{\eta\eta}z_{\xi} - x_{\xi}y_{\eta}z_{\xi\eta} \end{aligned} \quad (A5)$$

$$\begin{aligned} \frac{\partial|J|}{\partial\zeta} = & x_{\xi\xi}y_{\eta}z_{\xi} + x_{\xi}y_{\eta\xi}z_{\xi} + x_{\xi}y_{\eta}z_{\xi\xi} - x_{\eta\xi}y_{\xi}z_{\xi} - x_{\eta}y_{\xi\xi}z_{\xi} - x_{\eta}y_{\xi}z_{\xi\xi} \\ & - x_{\xi\xi}y_{\xi}z_{\eta} - x_{\xi}y_{\xi\xi}z_{\eta} - x_{\xi\xi}y_{\xi}z_{\eta\xi} + x_{\xi\xi}y_{\xi}z_{\eta} + x_{\xi}y_{\xi\xi}z_{\eta} + x_{\xi}y_{\xi}z_{\eta\xi} \\ & + x_{\eta\xi}y_{\xi}z_{\xi} + x_{\eta}y_{\xi\xi}z_{\xi} + x_{\eta}y_{\xi}z_{\xi\xi} - x_{\xi\xi}y_{\eta}z_{\xi} - x_{\xi}y_{\eta\xi}z_{\xi} - x_{\xi}y_{\eta}z_{\xi\xi} \end{aligned} \quad (A6)$$